DTIC COPY

REPORT DOCUMENTATION PAGE

Form Approved
OMB No. 0704-01-0188

PLEASE DO NOT RETURN YOUR FORM TO THE ABOVE ADDRESS.

1. REPORT DATE (DD-MM-YYYY)	2. REPORT TYPE	3. DATES COVERED (From - To)
22-09-2007	REPRINT	

4. TITLE AND SUBTITLE

Global MHD test particle simulations of >10 MeV radiation belt electrons during sudden storm commencement

5a. CONTRACT NUMBER

5b. GRANT NUMBER

5c. PROGRAM ELEMENT NUMBER
62601F

6. AUTHORS
B.T. Kress*, M.K. Hudson*, M.D. Looper**, J. Albert, J.G. Lyon # and C.C. Goodrich#

5d. PROJECT NUMBER
1010

5e. TASK NUMBER
RS

5f. WORK UNIT NUMBER
A1

7. PERFORMING ORGANIZATION NAME(S) AND ADDRESS(ES)

Air Force Research Laboratory /RVBXR
29 Randolph Road
Hanscom AFB, MA 01731-3010

8. PERFORMING ORGANIZATION REPORT NUMBER
AFRL-RV-HA-TR-2008-1012

9. SPONSORING/MONITORING AGENCY NAME(S) AND ADDRESS(ES)

10. SPONSOR/MONITOR'S ACRONYM(S)
AFRL/RVBXR

11. SPONSOR/MONITOR'S REPORT NUMBER(S)

12. DISTRIBUTION/AVAILABILITY STATEMENT
Approved for Public Release; distribution unlimited.

13. SUPPLEMENTARY NOTES
Reprinted from Journal of Geophysical Research, Vol. 112, A09215, doi:10.1029/2006JA012218, 2007 ©2007, American Geophysical Union.
* Dartmouth College, Hanover, NH. **Aerospace Corp., Los Angeles, CA #Boston University, Boston, MA

14. ABSTRACT

Prior to 2003, there are two known cases where ultrarelativistic (≥ 10 MeV electrons appeared in the Earth's inner zone radiation belts in association with high speed interplanetary shocks: the 24 March 1991 and the less well studied 21 February 1994 storms. During the March 1991 event electrons were injected well into the inner zone on a timescale of minutes, producing a new stably trapped radiation belt population that persisted for ~10 years. More recently, at the end of solar cycle 23, a number of violent geomagnetic disturbances resulted in large variations in ultrarelativistic electrons in the inner zone, indicating that these events are less rare than previously thought. Here we present results form a numerical study of shock-induced transport and energization of outer zone electrons in the 1-7 MeV range, resulting in a newly formed 10-20 MeV electron belt near L ~ 3. Test particle trajectories are followed in time-dependent fields from an MHD magnetospheric model simulation of the 29 October storm sudden commencement.

15. SUBJECT TERMS

Pitch angle diffusion | Radiation belts | Energetic electrons

16. SECURITY CLASSIFICATION OF:			17. LIMITATION OF ABSTRACT	18. NUMBER OF PAGES	19a. NAME OF RESPONSIBLE PERSON
a. REPORT	b. ABSTRACT	c. THIS PAGE			J. M. Albert
UNCL	UNCL	UNCL	Unl	15	19B. TELEPHONE NUMBER (Include area code)

JOURNAL OF GEOPHYSICAL RESEARCH, VOL. 112, A09215, doi:10.1029/2006JA012218, 2007

Global MHD test particle simulations of >10 MeV radiation belt electrons during storm sudden commencement

B. T. Kress,[1] M. K. Hudson,[1] M. D. Looper,[2] J. Albert,[4] J. G. Lyon,[3] and C. C. Goodrich[3]

Received 8 December 2006; revised 8 May 2007; accepted 7 June 2007; published 22 September 2007.

[1] Prior to 2003, there are two known cases where ultrarelativistic (≳10 MeV) electrons appeared in the Earth's inner zone radiation belts in association with high speed interplanetary shocks: the 24 March 1991 and the less well studied 21 February 1994 storms. During the March 1991 event electrons were injected well into the inner zone on a timescale of minutes, producing a new stably trapped radiation belt population that persisted for ~10 years. More recently, at the end of solar cycle 23, a number of violent geomagnetic disturbances resulted in large variations in ultrarelativistic electrons in the inner zone, indicating that these events are less rare than previously thought. Here we present results from a numerical study of shock-induced transport and energization of outer zone electrons in the 1–7 MeV range, resulting in a newly formed 10–20 MeV electron belt near $L \sim 3$. Test particle trajectories are followed in time-dependent fields from an MHD magnetospheric model simulation of the 29 October 2003 storm sudden commencement (SSC) driven by solar wind parameters measured at ACE. The newly formed belt is predominantly equatorially mirroring. This result is in part due to an SSC electric field pulse that is strongly peaked in the equatorial plane, preferentially accelerating equatorially mirroring particles. The timescale for subsequent pitch angle diffusion of the new belt, calculated using quasi-linear bounce-averaged diffusion coefficients, is in agreement with the observed delay in the appearance of peak fluxes at SAMPEX in low Earth orbit. We also present techniques for modeling radiation belt dynamics using test particle trajectories in MHD fields. Simulations are performed using code developed by the Center for Integrated Space Weather Modeling.

Citation: Kress, B. T., M. K. Hudson, M. D. Looper, J. Albert, J. G. Lyon, and C. C. Goodrich (2007), Global MHD test particle simulations of >10 MeV radiation belt electrons during storm sudden commencement, *J. Geophys. Res.*, *112*, A09215, doi:10.1029/2006JA012218.

1. Introduction

[2] In comparison with the Earth's outer zone radiation belts, sudden large variations in the inner zone energetic particle fluxes ($L \lesssim 3$) are rare, occurring only during very large geomagnetic storms, usually initiated by coronal mass ejection (CME) driven interplanetary shocks. This contrast is especially evident for very energetic particles (≳10 MeV) which have long radial diffusion and loss timescales allowing stably trapped electron and ion belts to persist for months to years. To illustrate, Figure 1 shows a summary plot of daily averages of 10–20 MeV electron count rates versus L-shell (L) from the Proton/Electron Telescope (PET) on the Solar Anomalous and Magnetospheric Particle Explorer (SAMPEX) spacecraft. The plot shows 10–20 MeV electron count rates from the start of the SAMPEX mission in July 1992 through September 2005. The heightened fluxes near $L \sim 2$, present at the beginning of the SAMPEX mission, are the remnants of the 24 March 1991 CME-driven interplanetary shock that compressed the magnetopause inside geosynchronous orbit injecting electrons well into the inner zone on a timescale of minutes [*Blake et al.*, 1992]. The first significant enhancement following the March 1991 storm appearing in Figure 1 is associated with the 21 February 1994 storm. A strong ground-based SSC was observed by low-latitude magnetometers for this event (K. Shiokawa, private communication, 2005), roughly half the amplitude of the March 1991 SSC which was the strongest on record [*Araki et al.*, 1997]. This event was followed by a long period of relatively little change during solar minimum, between solar cycles 22 and 23, characterized by the slow radial diffusion and loss timescales evident in the plot. The violent geomagnetic storms of October–November 2003 mark the beginning of the strong activity characterizing the declining phase of the solar cycle. During the "Halloween storm," ultrarelativistic electrons were injected well inside of $L \sim 3.5$ producing a stably trapped

[1]Department of Physics and Astronomy, Dartmouth College, Hanover, New Hampshire, USA.
[2]Space Sciences Department, Aerospace Corporation, Los Angeles, California, USA.
[3]Center for Integrated Space Weather Modeling, Boston University, Boston, Massachusetts, USA.
[4]Space Vehicles Directorate, Air Force Research Laboratory, Hanscom Air Force Base, Massachusetts, USA.

0148-0227/07/2006JA012218$09.00

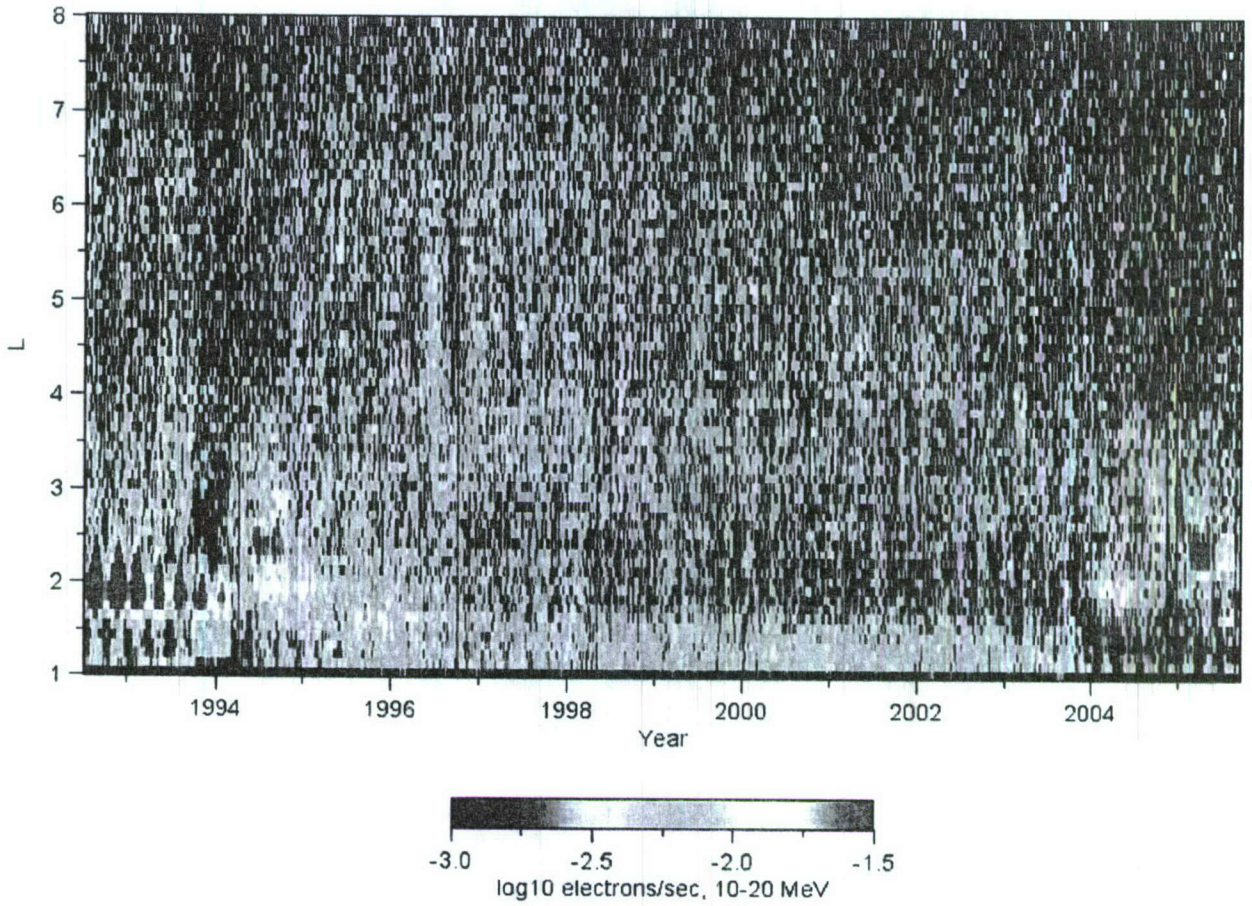

Figure 1. Daily averages of 10–20 MeV electron count rates from the PET instrument on SAMPEX from July 1992 through September 2005. A new belt injected during the 29 October 2003 storm appears as a weak enhancement near $L = 2$ beginning $\sim$ February 2004.

radiation belt population that persisted for several months [*Looper et al.*, 2005]. This belt appears in Figure 1 as a weak enhancement in fluxes near $L = 2$ beginning $\sim$ February 2004; and it is evident in the expanded Figure 4 of Looper et al. that weak fluxes, just above background level, extend back in time to October–November 2003. Looper et al. attribute the ~4 month delay in the appearance of peak fluxes at SAMPEX (in low Earth orbit) to a slow pitch angle diffusion from a population initially mirroring near the equatorial plane. Looper et al. also note that >10 MeV electrons injected during the 24 March 1991 storm observed by the Combined Release and Radiation Effects Satellite (CRRES) (in near equatorial orbit) had an equatorial pitch angle distribution strongly peaked near 90°, suggesting that a similar physical mechanism is responsible for the newly formed belt in each case. Several additional enhancements are seen in Figure 1, after the beginning of 2004, associated with November 2004, January 2005, and May 2005 storms.

[3] For comparison, Figure 2 shows 2–6 MeV electron count rates versus L (bottom) and 10–20 MeV electron count rates versus L (top), both from the PET instrument on SAMPEX (i.e., the top of Figure 2 is an expanded version of Figure 1 over the 9 month period following 1 October 2003). A new belt of 2–6 MeV electrons appears in and below the

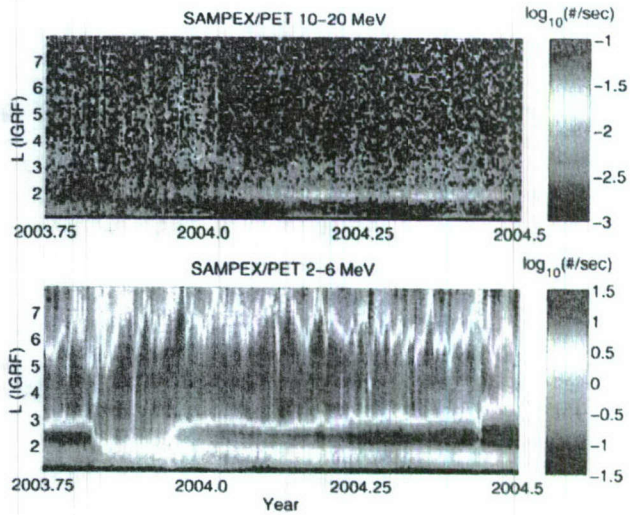

Figure 2. (top) The 10–20 MeV electron count rate from the PET instrument on SAMPEX from 1 October 2003 to 1 July 2004. The vertical red line at 29 October 2003 is a large solar energetic electron event [*Looper et al.*, 2005]. (bottom) The 2–6 MeV electron flux from the PET instrument on SAMPEX with the same timescale as above.

slot region 1–3 days following the 29 October 2003 storm onset [*Baker et al.*, 2004]. This newly formed 2–6 MeV belt has been attributed both to adiabatic energization and transport due to strongly enhanced magnetospheric ultra-low frequency (ULF) waves [*Loto'aniu et al.*, 2006] and to local heating by whistler mode chorus waves [*Horne et al.*, 2005a, 2005b; *Shprits et al.*, 2006]. The striking difference in timescales and location of the appearance of Halloween storm electrons for these different energy ranges suggest that a different physical process is responsible for the formation of new belts in each case.

[4] A mechanism that has been investigated previously, in connection with the formation of new energetic electron and ion belts, is the inward transport and adiabatic acceleration of outer zone electrons by an electric field pulse launched when an interplanetary shock impacts the magnetosphere. The inductive SSC electric field pulse accompanies an increase in the magnetic field measured by spacecraft and ground magnetometers. The leading portion of the bipolar electric field pulse can exceed ~100 mV/m [*Wygant et al.*, 1994] and is predominantly westward. Energetic electrons in drift resonance with the azimuthally propagating SSC electric field pulse can $\mathbf{E} \times \mathbf{B}$ drift inward through several L-shells, undergoing significant energization in a fraction of a drift period due to conservation of the first adiabatic invariant. *Li et al.* [1993] modeled the formation of a new electron belt at $L \sim 2.5$ during the 24 March 1991 storm by following electron guiding centers restricted to the equatorial plane in a pure dipole magnetic field traversed by an analytically modeled bipolar electric field pulse. The model was found to reproduce the observed electron drift echoes well. *Hudson et al.* [1995] used the same technique to model the formation of a new proton radiation belt at $L \sim 2.5$, also observed during the March 1991 event [*Blake et al.*, 1992]. *Hudson et al.* [1997] used an MHD-guiding center test particle simulation of the March 1991 storm, again restricted to equatorial plane particle dynamics, to simulate the formation of a new proton belt earthward of solar energetic proton penetration. *Elkington et al.* [2004] applied similar techniques to electrons, reproducing the flux peak in energy at 13 MeV and $L \sim 2.5$ which was the signature of prompt injection on a drift timescale in the CRRES measurements. A recent parametric study by *Gannon et al.* [2005] investigated the shock-induced transport and energization of relativistic electrons in the magnetosphere using the Li et al. model. Gannon et al. studied the location and intensity of new belts for a variety of electric field pulse propagation velocities and amplitudes in the range from 750 to 2500 km/s and 120 to 240 mV/m and found that a pulse speed $\gtrsim$1200 km/s is required to produce significant flux levels in the new belt, also that a pulse amplitude $\gtrsim$120 mV/m is required to form a new belt inside of $L \sim 3$.

[5] Similarities between the March 1991 event and subsequent injections of >10 MeV electrons shown in Figure 1 lead us to consider the possibility that these additional enhancements are also prompt shock-induced injections due to transport and energization by the SSC electric field pulse associated with each event. The 21 February 1994 event has been modeled in a separate study limited to equatorial plane guiding center test particle dynamics [*Hudson et al.*, 2006], with conclusions similar to the 24 March 1991 event modeled by *Elkington et al.* [2002]. In the present study of the 29 October 2003 event, we use an MHD magnetospheric model to simulate an ~5 min period during and immediately after the arrival of the interplanetary shock that initiated the storm. Test particle trajectories are followed in MHD fields to investigate the appearance of >10 MeV electrons at $L \sim 2$. The inner boundary conditions used in the MHD model at $L \sim 2$, however, restricts inward particle transport at/near the inner boundary, limiting this study to regions $L \gtrsim 2$. One question we address is why one would expect the resulting new belt to have a pitch angle distribution strongly peaked near 90° as indicated by observations; thus it is necessary to simulate three-dimensional (3-D) particle dynamics not restricted to the equatorial plane.

[6] In section 2 we present techniques used for global modeling of radiation belt dynamics using three-dimensional test particle trajectories in MHD fields, including a novel method of obtaining modeled fluxes that one would expect to measure with a spacecraft detector. In section 3 we present global MHD, test particle, and pitch angle diffusion results. Finally, we conclude with a summary and discussion in section 4.

2. Global MHD Test Particle Numerical Model

2.1. Test Particle Integrations in MHD Fields

[7] An energetic particle distribution in the magnetosphere can be modeled by following weighted Lorentz and/or guiding center test particle trajectories in time-dependent MHD model fields; thus, the full kinetic effects of particle interactions with MHD magnetospheric physics is included. Since the total energy density of MeV ions and electrons in the magnetosphere is very small compared to the thermal population, these particles may be considered noninteracting, justifying a test particle approach [*Dessler and Parker*, 1959; *Sckopke*, 1966].

[8] Test particle trajectories are integrated using a fourth-order Runge-Kutta integrator. Fast integration of Lorentz and guiding center trajectories is performed by linearly interpolating magnetic and electric fields from a four dimensional (x, y, z, t) grid to particle or guiding center positions at each time step. Since a Lorentz trajectory involves timescales several orders of magnitude smaller than a guiding center trajectory, for computational efficiency it is desirable to compute the latter. However, MeV particles in the solar wind and outer magnetosphere frequently do not conserve their first adiabatic invariant. In this case it is necessary to follow the full Lorentz motion of the particle, and we compute a particle trajectory by solving the relativistic Lorentz equation

$$\frac{d(\gamma \mathbf{v})}{dt} = \frac{q}{m}\left(\mathbf{E} + \frac{\mathbf{v}}{c} \times \mathbf{B}\right), \tag{1}$$

where $\mathbf{v}$ is the velocity of a particle with charge q and mass m, $\gamma = 1/\sqrt{1 - v^2/c^2}$ is the relativistic factor, and c is the speed of light.

[9] If the gyroperiod of a particle is much smaller than the timescale on which local electric and magnetic fields evolve and the particle gyroradius is much smaller than the scale

length of local variations in the fields, then the first adiabatic invariant is conserved by the particle orbit, and we may use the guiding center equations to advance the gyroaveraged center of the particle position. The relativistic guiding center equations are

$$\mathbf{v}_d = \frac{c\hat{b}}{Bq} \times \left[-qE + \frac{M}{\gamma} \nabla B + \frac{p_\parallel^2}{\gamma m} \left(\hat{b} \cdot \nabla \right) \hat{b} \right], \tag{2}$$

$$\dot{p}_\parallel = \left[qE_\parallel - \frac{M}{\gamma} \left(\hat{b} \cdot \nabla \right) B \right], \tag{3}$$

$$\frac{p_\perp^2}{2mB} = M = \text{a constant}, \tag{4}$$

where $\mathbf{v}_d$ is the guiding center drift velocity, $p_\parallel$ and $p_\perp$ are the parallel and perpendicular components of the relativistic particle momentum, and the first adiabatic invariant M is a conserved quantity. The brackets on the right-hand side of equations (2) and (3) contain the electric field force $\mathbf{F}_E$, the gradient drift force term $\mathbf{F}_{\nabla B}$, the curvature force term $\mathbf{F}_{\text{curv}}$, and the mirror force $\mathbf{F}_{\text{mirror}}$ [*Northrop*, 1963].

[10] When using linearly interpolated fields, standard adaptive stepsize integrators fail due to lack of continuous first- and higher-order spatial derivatives at grid cell boundaries. For example, the *Press et al.* [1992] fourth-order Runge-Kutta quality-controlled rkqc routine uses the difference between fourth- and fifth-order approximations to obtain an error approximation for adapting the time step. An alternative method, used to integrate a Lorentz trajectory, is to set the time step to ~1/100th the instantaneous particle gyroperiod [e.g., *Smart et al.*, 2000]. A locally determined guiding center time step is more problematic however, (1) due to discontinuities in the linearly interpolated magnetic fields at grid cell boundaries, (2) since the velocity goes to zero at a mirror point, and (3) since the mirror force goes to zero in the magnetic equatorial plane. We employ a guiding center adaptive stepsize that uses the instantaneous guiding center drift force terms to set Δt at each time step. A locally determined adaptive time step for integrating the guiding center equations is

$$\Delta t = \epsilon \frac{p}{|\mathbf{F}_E + \mathbf{F}_{\nabla B} + \mathbf{F}_{\text{curv}} + \mathbf{F}_{\text{mirror}}|}, \tag{5}$$

where p is the total particle momentum and ϵ is a small parameter numerically determined to accurately integrate a guiding center trajectory. We find that $\epsilon \sim 0.1$ gives accurate results (e.g., $\lesssim$1% error for bounce and drift times in a dipole and to within 1% of a converged upon solution in arbitrary fields). In arbitrary fields where all the guiding center force terms may go to zero, e.g., in the solar wind, a maximum time step size should also be used, e.g., $\Delta t = \min(\Delta t, \Delta \mathbf{x}_{\max}/\mathbf{v}_d)$.

[11] An adiabaticity or "epsilon" parameter, which characterizes the length scale of variations in the magnetic field with respect to a particle gyroradius ρ_{gyro}, is used to determine the validity of the guiding center approximation:

$$\epsilon = \rho_{\text{gyro}} \frac{|\nabla \mathbf{B}|}{B}. \tag{6}$$

Here $|\nabla \mathbf{B}|$ is a norm of the $\nabla \mathbf{B}$ tensor (see Appendix A). This number is used as a switch, to go between guiding center and Lorentz trajectories when appropriate. We find numerically that when $\epsilon \lesssim 0.05$ there is good agreement between guiding center and Lorentz methods over a drift period. When $\epsilon \gtrsim 0.05$, a trajectory is switched from a guiding center to a Lorentz trajectory using a randomly chosen gyrophase angle. When $\epsilon \lesssim 0.01$, a Lorentz trajectory is switched to a guiding center trajectory.

[12] In the work presented here, all particles are initiated with guiding center trajectories, and most remain in the guiding center mode throughout the simulation. Of the few that are switched to the Lorentz mode, most are switched when they encounter the magnetopause and are subsequently lost to the outer boundary.

2.2. Initializing the Test Particle Distribution

[13] The computational domain for energetic particle trajectory tracing consists of a sphere centered on the Earth with radius $r \sim 15\ R_E$ (Earth radii) located well inside the MHD magnetospheric model outer boundary. The dayside magnetopause in the MHD model is inside of the sphere, while the magnetotail cuts through the sphere boundary on the nightside. Particles exiting the sphere are removed from the simulation. There is also an inner boundary at $\sim 2\ R_E$ which is the inner boundary of the MHD magnetospheric model fields. Particles striking this inner boundary are also removed from the simulation.

[14] To initialize an outer radiation belt population, particles are launched randomly and uniformly from a disk in the equatorial plane with random uniform distributions in equatorial pitch angle and energy. To avoid an initial bounce phase bunching, launch times are distributed over a presimulation time interval greater than the longest particle bounce period. Particles are launched with energies from 1 to 7 MeV and between radial distances at 3 and 8 R_E. The limits of the initial equatorial pitch angle distribution are determined by the local-time dependent loss cone in the initial MHD model fields, and are limited to $\gtrsim 35°$ and $\lesssim 145°$ by the inner boundary of the MHD model at $\sim 2\ R_E$.

[15] The exact nature of the initial test particle distribution is not important except that we wish to sample the phase space we are interested in fully and in an approximately uniform way. The initial distribution is subsequently weighted, in a postprocessing step, using an appropriate observed or model distribution which is to be used as the initial condition. The particle weights are then used to obtain the fluxes one would expect to measure with a spacecraft detector. The energy and radial limits of the initial test particle distribution are determined by the radiation belt model used to weight the particles. In this work we use the European Space Agency (ESA) CRRES radiation belt electron model [*Vampola*, 1996], obtained from CRRES data. The model fluxes used are defined on an L-energy grid from $L = 3$ to 8 and $E = 1$ to 7 MeV. Particles are initially launched in this range. Any particles initially

outside of these limits would receive a particle weight of zero and would not contribute to the weighted particle flux for the remainder of the simulation.

2.3. Numerically Determined Flux

[16] Particle fluxes are measured directly in the code using a numerical detector. The detector is a disk in the equatorial plane. Test particle flux is measured by counting particles as they pass through the disk and binning the results in position, energy, and equatorial pitch angle space ($\mathbf{x}_i$, T_j, α_{ok}). The flux integration time δt is chosen $\lesssim \tau_{b\min}$, the smallest particle bounce period, so that we do not over sample a subset of the trajectories with small bounce periods. For this work $\delta t \sim 0.05$ s.

[17] The directional flux entering a detector is in general a function of position $\mathbf{x}$, direction of incidence $\hat{\mathbf{u}}$, kinetic energy T, and time t, and may be determined using

$$j(\mathbf{x}, \hat{\mathbf{u}}, T, t) = \frac{\delta N}{\delta A \ \cos\theta \ \delta\Omega \ \delta T \ \delta t}, \tag{7}$$

where δN is the number of particles striking a surface of area δA with directions of incidence lying inside solid angle $\delta\Omega$ oriented along the unit vector $\hat{\mathbf{u}}$, with kinetic energies in the interval δT, during the time interval δt. θ is the angle between the normal to δA and the $\hat{\mathbf{u}}$ direction [*Roederer*, 1970, pp. 85–86]. If the distribution is uniform in gyrophase, the direction of incidence of the particles will only be a function of pitch angle α. In this case the solid angle $\delta\Omega$ can be expressed as $2\pi \sin\alpha \ \delta\alpha$. If we further assume that in the equatorial plane $\alpha \approx \theta$, which is usually true to within ~1% for trapped particles in the MHD model fields, the directional flux in the *ijk*th bin, with *i*, *j*, and *k* indexing position, kinetic energy, and equatorial pitch angle, respectively, may be obtained from the code using

$$j(\mathbf{x}_i, T_j, \alpha_{o_k}) = \frac{\sum_{\substack{\text{Number of flux} \\ \text{counts in } ijk^{\text{th}} \text{ bin}}} w_n}{\delta A_i \ \cos\alpha_k \ 2\pi \ \sin\alpha_k \ \delta\alpha_k \ \delta T_j \ \delta t}, \tag{8}$$

where w_n is the particle weight (defined below). Note that there is a zero in the denominator for equatorially mirroring particles. This difficulty is removed by choosing equatorial pitch angle bins on either side of $\alpha_o = 90°$. For simplicity, equation (8) is an expression for 0th order binning of particle flux counts, i.e., equivalent to the nearest grid point (NGP) method. A linear weighting, which also includes a grid weighting factor for interpolating flux counts to ($\mathbf{x}_i$, T_j, α_{o_k}) grid points, is used in the code to reduce noise in the resulting distribution function.

2.4. Particle Weighting

[18] As a postprocessing step, test particles are weighted with an observed or model flux distribution that is chosen to serve as initial conditions. The test particle flux counts are collected in a file at specified dump times during the simulation and then used along with their corresponding particle weights to compute model fluxes that would be measured by a spacecraft detector throughout the simulation.

[19] The particle weights are determined as follows. Near the start of the simulation, test particle fluxes are binned on the same grid that the weighting model's flux distribution is specified on, to obtain an initial test particle flux $j_{\text{test particle}}(t = 0)$. The test particle flux is measured by setting all particle weights $w_n = 1.0$ in equation (8) above. The initial test particle flux is measured in the code after a time interval greater than the longest test particle drift period, in order to remove particles that were initiated in the bounce and drift loss cones.

[20] The particle weighting function is determined by

$$w(L_i, T_j, \alpha_{o_k}) = \frac{j_{\text{model}}(L_i, T_j, \alpha_{o_k})}{j_{\text{test particle}}(L_i, T_j, \alpha_{o_k}; t = 0)}. \tag{9}$$

When weighting particles, the weighting function, model fluxes, and initial test particle fluxes are all defined on the same grid. Each particle is given a weight $w_n = w(L_n, T_n, \alpha_{o_n}; t = 0)$. The particle weights may be simply interpreted as the number of particles per test particle [e.g., see *Hockney and Eastwood*, 1988, pg. 27]. Each particle retains its weight throughout the simulation, thereby preserving the total number of particles along its trajectory. At later times during the simulation, we are not restricted to fluxes defined in terms of the initial model distribution phase space variables, e.g., particles with an initial flux distribution defined in terms of L, T, and α_o may at later times during the simulation be used to yield information about $j(\mathbf{x}, T, \alpha_o)$ on a different grid than the one used for weighting.

[21] A number of approximations have been made in the initial test particle weighting used in this work: (1) For simplicity, the model L-shell is interpreted as dipole L, i.e. radial distance in the equatorial plane, rather than using McIlwain L determined in quiet Olsen-Pfitzer model fields, which was originally used to sort CRRES observations. (2) The equatorial pitch angle flux distribution is initially assumed to be flat between 35° and 145° and zero outside this range. Note that one of our present goals is to isolate the effect on the pitch angle distribution of particles accelerated by the SSC electric field pulse. Since outer zone electrons usually have a maximum in their equatorial pitch angle distribution near 90°, we expect the degree to which the final distribution is peaked near 90° to be underestimated by the assumption of an initially flat pitch angle distribution. Also, this assumption is plausible; e.g., see *Seki et al.* [2005, Figure 5] which shows little variation in ~1 MeV electron fluxes with respect to equatorial pitch angle near $L \sim 4$ for equatorial pitch angles >45° and <135°. (3) Most importantly, the ESA model was produced using time averaged CRRES fluxes. We do not attempt to replicate the exact conditions preceding the 29 October 2003 event which are largely unknown but rather explore radiation belt dynamics under extreme conditions using plausible outer belt initial conditions.

3. Model Results

3.1. MHD Storm Sudden Commencement Electric Field

[22] In the following sections we present radiation belt model results obtained by following test particle trajectories in magnetohydrodynamic (MHD) model fields. The magnetic and electric fields are obtained from a global MHD simulation of the magnetosphere using the Lyon-Feder-

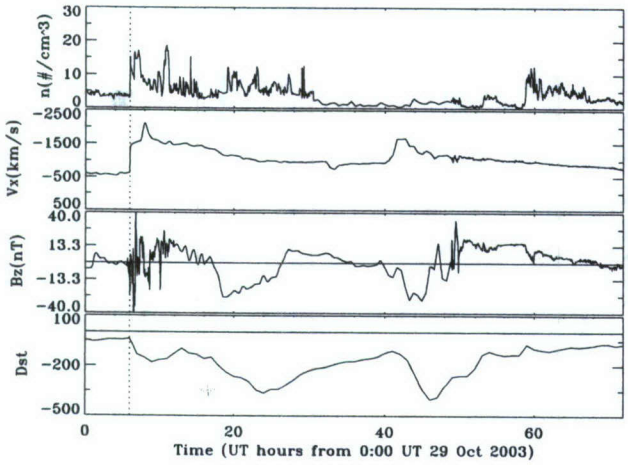

Figure 3. The 29–31 October 2003 ACE satellite data given in SM coordinates used to drive the LFM magnetospheric model. The Dst index from the Kyoto WDC Geomagnetic data service is also shown. The dashed line is at the 29 October 2003 SSC. The magnetic and velocity field components and plasma temperature, which are not shown, are also used as inputs to the MHD code.

Mobarry (LFM) code [*Lyon et al.*, 2004]. The solar wind density, velocity, temperature and magnetic field data from the Anomalous Composition Explorer (ACE) spacecraft were used to drive the MHD model at its sunward boundary. The 29 October 2003 solar wind density, velocity, and IMF B_z used as inputs to the code are shown in Figure 3. A high-resolution LFM simulation was performed with ~325 k grid points on a distorted spherical grid. The MHD time step was ~0.02 s. Field data was dumped at ~0.5 s intervals.

[23] An empirical plasmaspheric density model [*Gallagher et al.*, 1988], not usually included in the MHD model magnetosphere, was added to the MHD fields immediately preceding the arrival of the interplanetary shock at ~0600 UT on 29 October 2003. The LFM code does not contain physics necessary to model the evolution of the plasmasphere on longer timescales (~hours to days), i.e., a corotation electric field and cold plasma outflow source. The plasmaspheric density model is added to modify the Alfvén speed providing a more accurate description of SSC pulse propagation through the magnetosphere and the subsequent transient magnetospheric oscillations. The plasmasphere does not evolve significantly during the ~5 s interval simulated. The propagation of the SSC pulse through the inner magnetosphere is sensitive to the plasmasphere model density profile, which is parameterized in the model solely with the *Kp* index. A higher *Kp* reduces the plasmaspheric density and moves the plasmapause earthward in the model. *Kp* is fixed for a given 300 s run, i.e., the plasmasphere does not have time to evolve significantly on the SSC pulse propagation timescale. The same plasmasphere model was used in MHD-test particle simulations of the March 1991 event [*Hudson et al.*, 1997; *Elkington et al.*, 2002], with resulting particle fluxes in good agreement with CRRES proton and electron measurements.

[24] Figure 4 shows the azimuthal component of the SSC electric field pulse E_ϕ versus time at several points along the x-axis in solar magnetic (SM) coordinates, i.e., approximately along the day side Sun-Earth line. The pulse is shown for two separate LFM code runs with two different values of the *Kp* input parameter into the plasmaspheric model, with *Kp* = 3 (Figure 4a) and with *Kp* = 4 (Figure 4b). In each case, the initial E_ϕ displacement is in the westward (negative ϕ) direction, which can be understood by considering Faraday's law and a compression of the Earth's northwardly directed magnetic field. Thus the leading portion of the bipolar pulse shown in Figure 4 causes electrons and ions to $\mathbf{E} \times \mathbf{B}$ drift inward in *L*-shell. Particles in drift resonance with the azimuthal propagation of the pulse may be transported earthward several Earth radii, undergoing significant adiabatic energization. A rough estimate for the azimuthal propagation velocity of the pulse can be obtained by considering the time between the appearance of the pulse on the dayside at +3 R_E and on the nightside at −3 R_E. In the case with *Kp* = 3 this yields $3\pi R_E/60\text{s} \approx 1000$ km/s. In general, the effect of the addition of the plasmaspheric density is to slow, steepen, and intensify the SSC electric field pulse in the inner magnetosphere. On the day preceding the arrival of the 29 October 2003 CME, the *Kp* index fluctuated between *Kp* = 3 and *Kp* = 5 (Kyoto WDC Geomagnetic data service). On the morning of 29 October 2003, preceding the arrival of the shock, Kyoto WDC reported *Kp* = 4. Test particle results in fields from MHD runs using *Kp* = 3 and *Kp* = 4 are presented below. The case with *Kp* = 3 results in higher flux levels of >10 MeV electrons inside of $L \sim 3$ than the *Kp* = 4 case. MHD simulations with *Kp* = 2 and with no plasmaspheric density model were also performed (not shown). These additional runs follow the trend illustrated in Figure 4, i.e., an increased density in the inner magnetosphere produces a slower, narrower, and larger SSC electric field pulse. The case with no plasmasphere model included in the

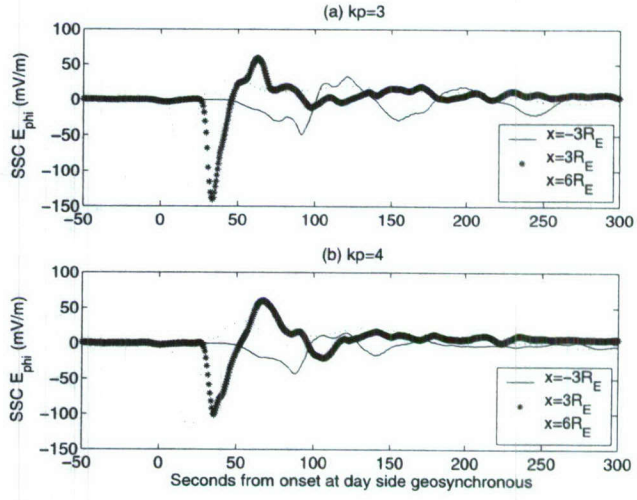

Figure 4. Azimuthal component of the MHD model SSC electric field pulse versus time at several points along the x-axis in solar magnetic (SM) coordinates, i.e., approximately along the Earth-Sun line. Results from two separate MHD magnetospheric model code runs are shown, with (a) *Kp* = 3 and (b) *Kp* = 4 used as input parameters into the plasmaspheric density model.

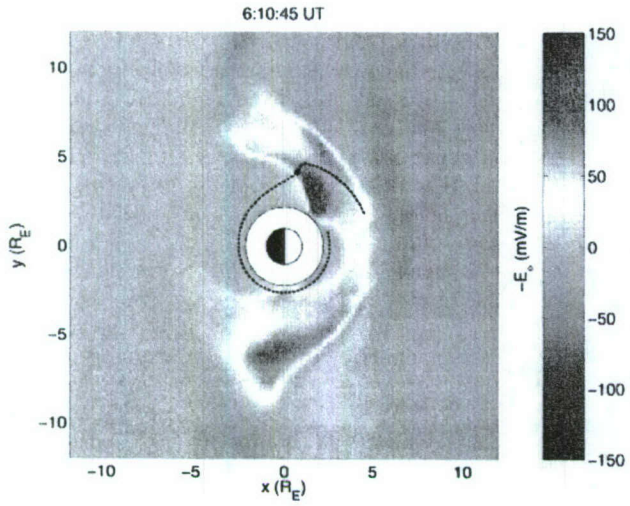

Figure 5. Time snapshot of the azimuthal component of the MHD model SSC electric field pulse in the equatorial plane. The dashed line shows the trajectory of a single adiabatically accelerated guiding center electron in drift resonance with the pulse as it propagates from the dayside to nightside. The initial and final energies of the particle are ~5 and 15 MeV, respectively.

MHD density produces a maximum electric field pulse of ~60 mV/m in the inner magnetosphere, which is not sufficient to produce a significant >10 MeV belt. The run with $Kp = 2$ produces a maximum electric field amplitude ~150 mV/m, only slightly larger than the run with $Kp = 3$.

[25] A time snapshot of E_ϕ in the equatorial plane is shown in Figure 5. Also shown in Figure 5 is the trajectory of a single guiding center electron that is in drift resonance with the pulse, moving with the crest of the pulse as it propagates from the dayside to nightside. The initial and final energies of the particle are ~5 and 15 MeV, respectively. The electron trajectory shown is equatorially mirroring (equatorial pitch angle is 90°). A meridional plot of the electric field magnitude (not shown) reveals that the SSC electric field pulse is mainly in the equatorial plane, thus preferentially accelerating equatorially mirroring particles which remain in the strongest portion of the pulse. This effect is enhanced by an additional focusing of the pulse into the equatorial plane as it enters the inner magnetosphere.This result is illustrated in Figure 6 which shows the SSC E_ϕ at two separate time snapshots as it enters the inner magnetosphere plotted in the noon-midnight meridional plane in solar magnetic (SM) coordinates. The pulse is focused into the equatorial plane as it enters the inner magnetosphere. In the inner magnetosphere, the pulse remains near the equatorial plane as it propagates toward the nightside.

3.2. Test Particle Model Results

[26] In each run, ~2.4 million test particle trajectories are computed during an ~5 min interval from the MHD simulation that includes the initial impact of the interplanetary shock on the magnetosphere at ~0600 UT, propagation of the resulting fast mode magnetosonic pulse through the magnetosphere, and during several large transient ULF oscillations following the arrival of the shock shown in Figure 4. An overview of the weighted test particle radiation belt results from the $Kp = 3$ case are shown in Figure 7. Omnidirectional integrated >10 MeV fluxes are plotted in the equatorial plane in SM coordinates at four snapshots in time from the simulation. Since the initial model distribution has no particles with energies above 7 MeV, there are initially zero >10 MeV fluxes. The initially localized injection appears at ~1500 local time. Figure 7 nicely illustrates the source of the drift echoes observed by a spacecraft particle detector [e.g., *Blake et al.*, 1992, Figure 1], i.e., a sudden appearance of heightened fluxes, with higher energy particles reaching the detector before lower energies due to a ∇B drift velocity dispersion of the initially localized injection. At a fixed location there is a gradual rise in fluxes as lower energies reach the detector until a sudden drop in fluxes occurs when the detector's lower-energy cutoff is reached. Subsequent drift echoes are gradually diminished by energy dispersion.

[27] Figure 8 shows 10 MeV equatorial pitch angle distributions in the newly formed belt ~5 min after storm onset. To produce the distributions, weighted particle fluxes are binned in dipole L-shell (radial distance in the equatorial plane), energy, and equatorial pitch angle. In the case with $Kp = 3$ the peak in 10 MeV flux occurs at $L \sim 3.0$, with the corresponding distribution shown in Figure 8b. Figure 8a shows the 10 MeV equatorial pitch angle distribution inside the flux peak, at $L \sim 2.5$. Figures 8c and 8d show distributions resulting from the run with $Kp = 4$, at the

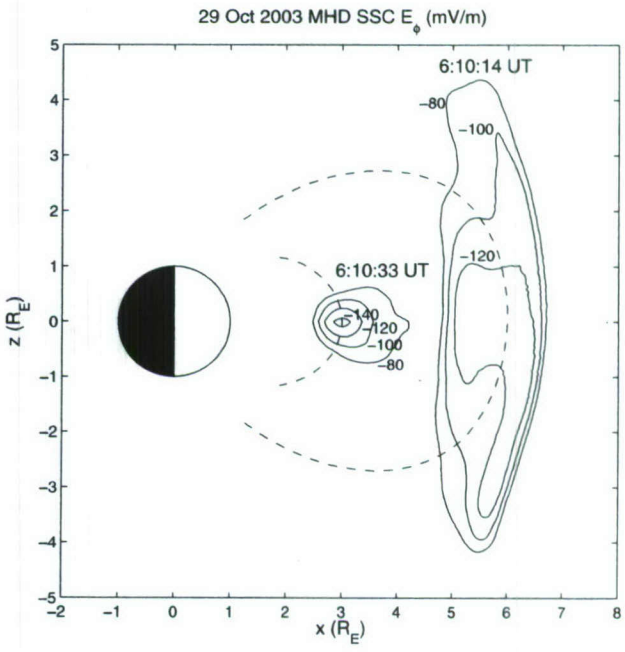

Figure 6. MHD E_ϕ peak at 6 R_E and at 3 R_E (two separate time snapshots) on the dayside in the noon-midnight meridional plane in solar magnetic (SM) coordinates. Contours from −80 to −140 mV/m in steps of −20 mV/m are shown. Dashed lines show magnetic field lines through $x = 6$ R_E and $x = 3$ R_E traced in the MHD fields in each respective time snapshot.

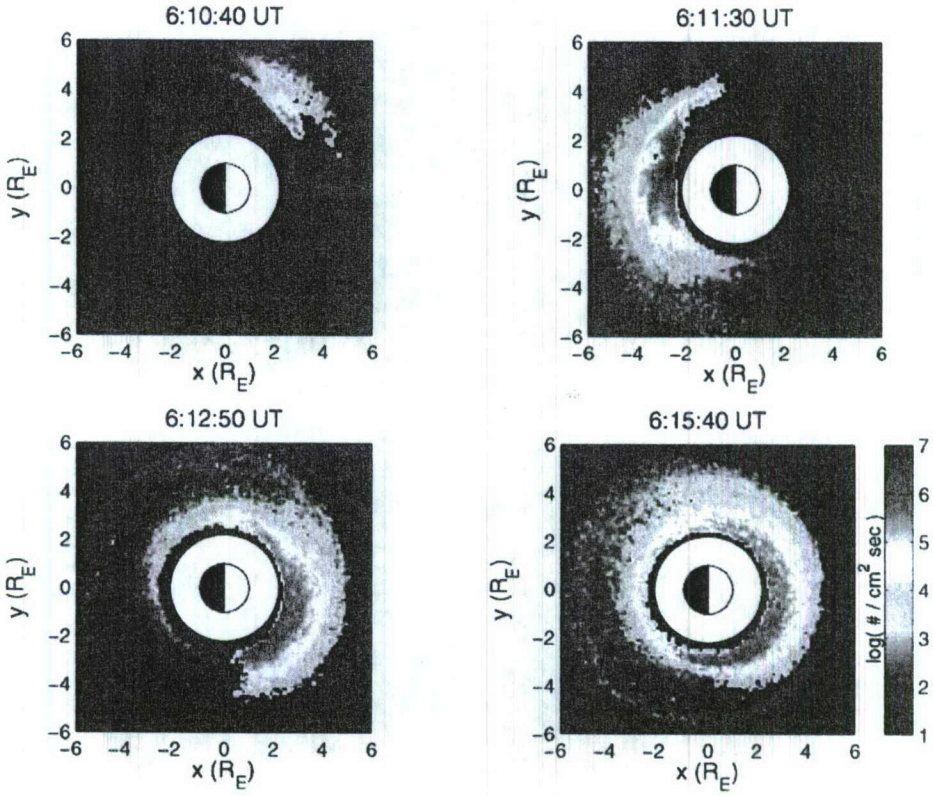

Figure 7. Integral omnidirectional fluxes of >10 MeV electrons in the equatorial plane in solar magnetic (SM) coordinates at four snapshots in time from the MHD test particle simulation, from the MHD magnetospheric model run using $Kp = 3$ as an input parameter to the plasmaspheric density model. The initial test particle distribution is weighted using the European Space Agency (ESA) CRRES radiation belt electron model [*Vampola*, 1996]. The model fluxes used for initial conditions are defined on an L-energy grid from $L = 3$ to 8 and $E = 1$ to 7 MeV; thus the initial >10 MeV flux in the model is zero.

location of the 10 MeV peak at $L \sim 3.5$, and inside the 10 MeV peak at $L \sim 3$. In each case, the solid line plot is a least squares fit to $A \sin^n(\alpha_o)$. The resulting distributions are strongly peaked around 90° with fluxes falling to zero near ±60°. Also note that the distributions become more peaked with decreasing L. The line plot shown in Figure 8b with $Kp = 3$ at 3.0 R_E is used as the initial condition for the pitch angle diffusion calculation presented in the next section.

3.3. Pitch Angle Diffusion

[28] An estimate for the timescale of the pitch angle diffusion of an equatorially mirroring population of radiation belt electrons, to a spacecraft position in low Earth orbit, may be obtained by solving a one-dimensional pitch angle diffusion equation. Bounce-averaged equatorial pitch angle diffusion coefficients are calculated according to quasi-linear theory in the high-density approximation [*Lyons*, 1974a, 1974b], using the computational techniques of *Albert* [1999] and the parameters of *Meredith et al.* [2006]. These values are based on CRRES data and successfully reproduced the observed decay times of 1.09 MeV electrons at $3 \leq L \leq 4$ and over a broader range in L for lower energies.

[29] The model has a density ratio $f_{pe}/f_{ce} = 8.9$ (corresponding to $n_e = 1086.6$) and a hiss amplitude of 34.5 pT. The power spectral density is a truncated Gaussian peaked at 550 Hz with width 300 Hz and lower and upper cutoffs at 100 Hz and 2000 Hz, respectively. The "small wavenormal model" is also a Gaussian (in $x = \tan\theta$), peaked at $x = 0$ with width $x_w = \tan 20°$, truncated at $\pm x_{\max} = \tan 30°$. Since, for high-energy particles, cyclotron resonance can occur with large harmonic numbers, n up to ±100 was kept, although most large n values are quickly eliminated by the computational procedure.

[30] The solid curve in Figure 9 shows the resulting diffusion coefficients for 10 MeV electrons, while the dashed curve shows 1 MeV values for comparison. The 10 MeV values were used to evolve the electrons in time according to the one-dimensional pitch angle diffusion equation

$$\frac{\partial f}{\partial t} = \frac{1}{T \sin\alpha_o \cos\alpha_o} \frac{\partial}{\partial \alpha_o} \left(D_{\alpha_o \alpha_o} T \sin\alpha_o \cos\alpha_o \frac{\partial f}{\partial \alpha_o} \right), \quad (10)$$

where T is the bounce period, with boundary conditions $f(\alpha_{o_{LC}}) = 0$ and $(df/da_o)_{\alpha_o} = 90° = 0$. The diffusion simulation was performed at $L = 3$ in a dipole, where the equatorial pitch angle at the edge of the loss cone is at ~8°. The initial distribution was modeled as $j = A \sin^n \alpha_o$ with $A = 40$, $n = 22$ (Figure 8b). Grid resolution was 1 degree, with timestep 10^{-4} days. The curves shown in Figure 10 are

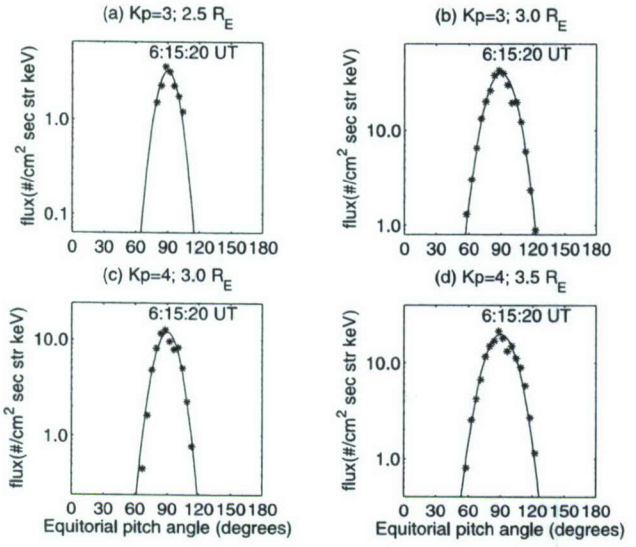

Figure 8. Equatorial pitch angle distributions of 10 MeV differential flux for various *Kp* and radial distances. The asterisks show nonzero fluxes obtained with equation (8) with 28 α_{o_i} bins uniformly spaced in cos α_o between 0 and 180 deg. The solid line is a least squares fit to $A \sin^n(\alpha_o)$ yielding: (a) $A = 3.2$, $n = 40$; (b) $A = 40$, $n = 22$; (c) $A = 12$, $n = 30$; (d) $A = 20$, $n = 18$. Note that in each figure, the axis has been scaled to span 2 decades and the maximum value of the flux has been located the same distance below the top of the vertical axis so that the rate the fluxes fall off from their maximum values can be compared.

snapshots over 200 days at increments of 10 days, starting from the dark blue curve. The flux takes 1 to 2 months to be discernable at the low equatorial pitch angles observable by SAMPEX at ~10 degrees (dashed line) and 3 to 4 months for the steady state pitch angle profile to be established, which is in agreement with the timescale for the delay in the appearance of peak flux levels at SAMPEX seen in Figure 1.

4. Summary and Discussion

[31] At energies in the 10s of MeV range the structure of the inner zone radiation belts is largely shaped by a few geomagnetic storms driven by high-speed interplanetary shock compressions of the magnetopause. The MHD test particle model results show that the 29 October 2003 SSC electric field pulse produces a new belt of >10 MeV electrons inside of $L \sim 3$ with an average quiet-time outer belt model source population assumed. The newly formed >10 MeV electron belt has its equatorial pitch angle distribution strongly peaked near 90° and becomes more peaked with lower L as shown in Figure 8. There are two primary reasons for the resulting peaked equatorial pitch angle distribution in the new belt: (1) The electrons are accelerated through conservation of the 1st adiabatic invariant perpendicular to the magnetic field increasing $p_\perp/p_\parallel$ and bringing their equatorial pitch angles closer to 90°, and (2) the SSC electric field pulse is predominantly in the equatorial plane, preferentially accelerating equatorially mirroring particles that spend more time in the pulse. The

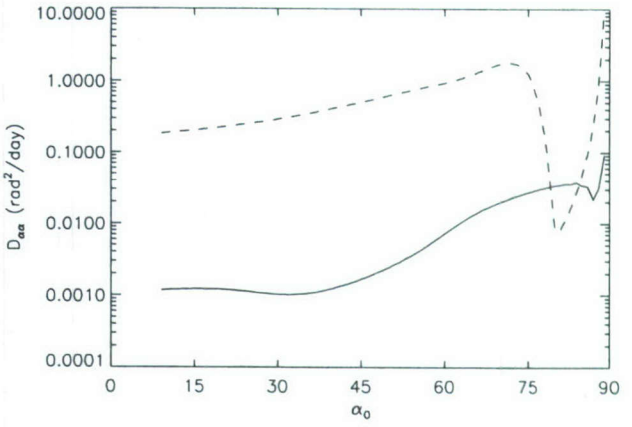

Figure 9. Bounce-averaged equatorial pitch angle diffusion coefficients calculated according to quasi-linear theory in the high density approximation [*Lyons*, 1974a, 1974b] using the computational techniques of *Albert* [1999] and parameters of *Horne et al.* [2005a, 2005b] (See text for model parameters). The solid curve shows the resulting diffusion coefficients for 10 MeV electrons, while the dashed curve shows 1 MeV values for comparison.

SSC electric field pulse is focused into the equatorial plane as it propagates into the plasmasphere, which has been added to the MHD fields immediately before the arrival of the shock using a *Kp*-dependent empirical density model. In general the effect of including a plasmaspheric density model in the MHD simulations is to enhance the amplitude of the SSC electric field pulse and decrease its speed in the inner magnetosphere. It is necessary to include a realistic plasmaspheric density in the MHD magnetospheric model to produce an SSC electric field pulse large enough to transport electrons over several L-shells producing a significant >10 MeV belt. This is consistent with *Gannon et al.* [2005] who find that an SSC E-field pulse ~10 mV/m

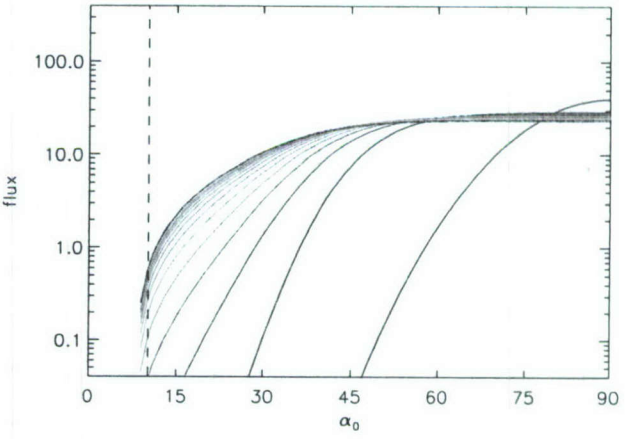

Figure 10. Equatorial pitch angle distribution of 10 MeV electrons evolved using (10) over 200 days at increments of 10 days, starting from the dark blue curve. The flux takes 1 to 2 months to be discernable at the low equatorial pitch angles observable by SAMPEX at ~10 degrees (dashed line) and 3 to 4 months for the steady state pitch angle profile to be established.

is more than an order of magnitude too small to produce a significant new belt with energies ~10 MeV. The delay, between the injection of >10 MeV electrons on 29 October 2003 and the appearance of peak flux levels at SAMPEX seen in Figure 1, indicates a pitch angle diffusion timescale ~ months which is in agreement with an estimate obtained by solving a one-dimensional pitch angle diffusion equation.

[32] On the basis of our results, we expect the location, energy, and equatorial pitch angle distribution of the newly formed belt to be dependent on the state of the outer zone electrons immediately preceding the SSC. In this work, we have not attempted to reproduce the exact state of the plasmasphere or outer electron belt preceding the 29 October 2003 event. Our main goal has been to study radiation belt dynamics under extreme conditions using a plausible initial state for the outer belt.

[33] It is not possible to make a direct comparisons with observation in this study, of the location and intensity of the newly formed radiation belt, since there was no satellite in near equatorial orbit capable of sampling the ultrarelativistic electrons as CRRES did during the 24 March 1991 event. However, the model does not produce a peak in >10 MeV electron flux near $L = 2$, where the new belt appears in the SAMPEX summary plot (Figure 1) several months following the 29 October 2003 storm. For example, in the case with $Kp = 3$ used as an input parameter to the plasmaspheric density model, the peak in 10 MeV flux forms at ~3 R_E. Peak fluxes at higher energies occur at lower L until the inner boundary of the MHD magnetospheric model is reached at ~2 R_E. The electric field pulse is modified in this region by the conditions imposed at the inner boundary on the MHD fields: the normal component of the magnetic flux through the inner boundary surface is held constant, and the normal component of the velocity at the inner boundary is zero, greatly diminishing the inductive electric field near the inner boundary and thereby reducing inward transport due to $\mathbf{E} \times \mathbf{B}$ drift near $L \sim 2$. The Courant condition on pulse propagation across a grid cell inhibits moving the inner boundary closer to Earth, where the Alfven speed is greater [*Lyon et al.*, 2004].

[34] While progress has been made with 2-D guiding center particle simulations modeling the 24 March 1991 injection, for which near equatorial plane measurements were available, we have since relied mainly on continuous low altitude polar orbiting spacecraft measurements in and near the loss cone. A number of storms subsequent to the March 1991 event show evidence of prompt shock-drift injections. *Blake et al.* [2005] examined the geoeffectiveness of shocks populating the radiation belts and found a correlation with sharp increase in the H-component, ground magnetometer perturbation which is the signature of an SSC event. The March 1991 event, two in November 2001 which produced trapping of solar energetic protons [*Kress et al.*, 2004, 2005; *Hudson et al.*, 2004; *Mazur et al.*, 2006], and both the 21 February 1994 and 28 October 2003 events appear to meet the criterion of producing a large inductive electric field pulse capable of transporting earthward to $L <$ 3 particles with azimuthal drift velocities comparable to the pulse propagation speed (~1000 km/s). CRRES electron data following the 24 March 1991 storm shows evidence of pitch angle distribution strongly peaked around 90° in the newly formed >10 MeV belt. A delay ~ months before the appearance of peak fluxes at LEO following the 21 February 1994 and 29 October 2003 storms suggest similarly peaked distributions, illustrating the need for an understanding of pitch angle evolution to model energetic particle fluxes in the radiation belts.

[35] The model results show that a quiet time outer zone electron distribution provides a source population for the observed injection, however, high fluxes of solar energetic particles were also present at the arrival of the interplanetary shock on 29 October 2003, with flux levels of solar energetic electrons in the 1–7 MeV range approaching those usually observed in the outer belts [*Mewaldt et al.*, 2005]. Solar energetic electrons (SEEs) provide a second possible source population for the newly formed 10–20 MeV electron belt. SEEs with a relativistic gamma factor $\gtrsim 10$ have gyroradii approaching the scale lengths of magnetic field gradients in the outer radiation belts, suggesting they may be promptly trapped in the magnetosphere as has previously been shown for solar energetic ions [*Kress et al.*, 2005; *Mazur et al.*, 2006]. We reserve for future investigation the role of SEEs as a source population for trapped >10 MeV electrons in the inner zone.

Appendix A: Nonadiabaticity

[36] The adiabaticity or "epsilon" parameter, used to determine the validity of the guiding center approximation, is frequently expressed

$$\varepsilon = \max\left(\left|\rho_{\text{gyro}}\frac{\nabla_\perp B}{B}\right|, \left|\rho_{\text{gyro}}\left(\hat{b}\cdot\nabla\right)\hat{b}\right|\right) \tag{A1}$$

However, in arbitrary three-dimensional fields this expression does not take into account magnetic rotational shear. As a simple example, consider the magnetic field

$$\mathbf{B} = \sin(nz)\hat{x} + \cos(nz)\hat{y}, \tag{A2}$$

for which $\varepsilon = 0$ for arbitrarily rapid variation in the $\hat{z}$ direction (i.e., arbitrarily large n). The field expressed by equation (A2) has no curvature or gradient in its magnitude, however, there is a rotational shear as we proceed in the $\hat{z}$ direction. Rotational shear is not uncommon in the magnetosphere and is produced at any place we find a current sheet; therefore in general we suggest a norm of the $\nabla\mathbf{B}$ tensor:

$$\varepsilon = \frac{\rho_{\text{gyro}}}{B}\sqrt{\sum_{i,j}\left(\frac{dB_i}{dx_j}\right)^2}, \tag{A3}$$

which captures all components of variations in the magnetic field (D. C. Montgomery, private communication, 2006).

[37] **Acknowledgments.** We thank our reviewers for many helpful comments and suggestions. Also, thank you to Chia-Lin Huang and Larry Kepko at Boston University for their help preparing the LFM solar wind input file. This material is based upon work supported in part by the STC Program of the National Science Foundation under agreement ATM-0120950.

[38] Amitava Bhattacharjee thanks Brian Anderson and Mei-Ching Fok for their assistance in evaluating this paper.

References

Albert, J. M. (1999), Analysis of quasi-linear diffusion coefficients, *J. Geophys. Res.*, *104*, 2429.

Araki, T., et al. (1997), Anomalous sudden commencement on March 24, 1991, *J. Geophys. Res.*, *102*, 14,075.

Baker, D. N., S. G. Kanekal, X. Li, S. P. Monk, J. Goldstein, and J. L. Burch (2004), An extreme distortion of the Van Allen belt arising from the 'Hallowe'en' solar storm in 2003, *Nature*, *432*, 878.

Blake, J. B., W. A. Kolasinski, R. W. Fillius, and E. G. Mullen (1992), Injection of electrons and protons with energies of tens of MeV into L > 4 on 24 March 1991, *Geophys. Res. Lett.*, *19*, 821.

Blake, J. B., P. L. Slocum, J. E. Mazur, M. D. Looper, R. S. Selesnick, and K. Shiokawa (2005), Geoeffectiveness of shocks in populating the radiation belts, in *Multiscale Coupling of Sun-Earth Processes*, edited by A. T. Y. Lui, Y. Kamide, and G. Consolini, pp. 125–135, Elsevier, New York.

Dessler, A. J., and E. N. Parker (1959), Hydromagnetic theory of magnetic storms, *J. Geophys. Res.*, *64*, 2239.

Elkington, S. R., M. K. Hudson, J. G. Lyon, and M. J. Wiltberger (2002), MHD particle simulations of radiation belt dynamics, *J. Atmos. Sol. Terr. Phys.*, *64*, 607.

Elkington, S. R., M. Wiltberger, A. A. Chan, and D. N. Baker (2004), Physical models of the geospace radiation environment, *J. Atmos. Sol. Terr. Phys.*, *66*, 1371.

Gallagher, D. L., P. D. Craven, and R. H. Comfort (1988), An empirical model of the Earth's plasmasphere, (COSPAR, IAGA, and SCOSTEP, Plenary Meeting, 27th, Symposium on Geospace Plasmas, 7th, Espoo, Finland, July 18–29, 1988), *Adv. Space Res.*, *8*, 15.

Gannon, J. L., X. Li, and M. Temerin (2005), Parametric study of shock-induced transport and energization of relativistic electrons in the magnetosphere, *J. Geophys. Res.*, *110*, A12206, doi:10.1029/2004JA010679.

Hockney, R. W., and J. W. Eastwood (1988), *Numerical Simulations Using Particles*, p. 27, A. Hilger, Philadelphia, Pa.

Horne, R. B., R. M. Thorne, S. A. Glauert, J. M. Albert, N. P. Meredith, and R. R. Anderson (2005a), Timescale for radiation belt electron acceleration by whistler mode chorus waves, *J. Geophys. Res.*, *110*, A03225, doi:10.1029/2004JA010811.

Horne, R. B., et al. (2005b), Wave acceleration of electrons in the Van Allen radiation belts, *Nature*, *437*, 227.

Hudson, M. K., A. D. Kotelnikov, X. Li, I. Roth, M. Temerin, J. Wygant, J. B. Blake, and M. S. Gussenhoven (1995), Simulations of proton radiation belt formation during the March 24, 1991 SSC, *Geophys. Res. Lett.*, *22*, 291.

Hudson, M. K., S. R. Elkington, J. G. Lyon, V. A. Marchenko, I. Roth, M. Temerin, J. B. Blake, M. S. Gussenhoven, and J. R. Wygant (1997), Simulations of proton radiation belt formation during storm sudden commencements, *J. Geophys. Res.*, *102*, 14,087.

Hudson, M. K., B. T. Kress, J. E. Mazur, K. L. Perry, and P. L. Slocum (2004), 3D modeling of shock-induced trapping of solar energetic particles in the Earth's magnetosphere, *J. Atmos. Sol. Terr. Phys.*, *66*, 1389.

Hudson, M. K., H. R. Mueller, B. T. Kress, V. Merkin, and J. B. Blake (2006), MHD-test particle modeling of prompt 10 MeV electron injection events, *Eos Trans. AGU*, *87*(36), Jt. Assem. Suppl., SM52A-02.

Kress, B. T., M. K. Hudson, K. L. Perry, and P. L. Slocum (2004), Dynamic modeling of geomagnetic cutoff for the 23–24 November 2001 solar energetic particle event, *Geophys. Res. Lett.*, *31*, L04808, doi:10.1029/2003GL018599.

Kress, B. T., M. K. Hudson, and P. L. Slocum (2005), Impulsive solar energetic ion trapping in the magnetosphere during geomagnetic storms, *Geophys. Res. Lett.*, *32*, L06108, doi:10.1029/2005GL022373.

Li, X., I. Roth, M. Temerin, J. R. Wygant, M. K. Hudson, and J. B. Blake (1993), Simulations of the prompt energization and transport of radiation belt particles during the March 24, 1991 SSC, *Geophys. Res. Lett.*, *20*, 2423.

Looper, M. D., J. B. Blake, and R. A. Mewaldt (2005), Response of the inner radiation belt to the violent Sun-Earth connection events of October–November 2003, *Geophys. Res. Lett.*, *32*, L03S06, doi:10.1029/2004GL021502.

Loto'aniu, T. M., I. R. Mann, L. G. Ozeke, A. A. Chan, Z. C. Dent, and D. K. Milling (2006), Radial diffusion of relativistic electrons into the radiation belt slot region during the 2003 Halloween geomagnetic storms, *J. Geophys. Res.*, *111*, A04218, doi:10.1029/2005JA011355.

Lyon, J. G., J. A. Fedder, and C. M. Mobarry (2004), The Lyon-Fedder-Mobarry (LFM) global MHD magnetospheric simulation code, *J. Atmos. Sol. Terr. Phys.*, *66*, 1333.

Lyons, L. R. (1974a), General relations for resonant particle diffusion in pitch angle and energy, *J. Plasma Phys.*, *12*, 45.

Lyons, L. R. (1974b), Pitch angle and energy diffusion coefficients from resonant interactions with ion-cyclotron and whistler waves, *J. Plasma Phys.*, *12*, 417.

Mazur, J. E., J. B. Blake, P. L. Slocum, M. K. Hudson, and G. M. Mason (2006), The creation of new ion radiation belts associated with solar energetic particles, *Geophys. Monogr. Ser.*, vol. 165, edited by N. Gopalswamy, R. Mewaldt, and J. Torsti, pp. 345–352, AGU, Washington, D.C.

Meredith, N. P., R. B. Horne, S. A. Glauert, R. M. Thorne, D. Summers, J. M. Albert, and R. R. Anderson (2006), Energetic outer zone electron loss timescales during low geomagnetic activity, *J. Geophys. Res.*, *111*, A05212, doi:10.1029/2005JA011516.

Mewaldt, R. A., C. M. S. Cohen, A. W. Labrador, R. A. Leske, G. M. Mason, M. I. Desai, M. D. Looper, J. E. Mazur, R. S. Selesnick, and D. K. Haggerty (2005), Proton, helium, and electron spectra during the large solar particle events of October–November 2003, *J. Geophys. Res.*, *110*, A09S18, doi:10.1029/2005JA011038.

Northrop, T. G. (1963), *The Adiabatic Motion of Charged Particles*, John Wiley, Hoboken, N. J.

Press, W. H., B. P. Flannery, S. A. Teukolsky, and W. T. Vetterling (1992), *Numerical Recipes in C: The Art of Scientific Computing*, 2nd ed., Cambridge Univ. Press, Cambridge, U. K.

Roederer, J. G. (1970), *Dynamics of Geomagnetically Trapped Radiation*, Springer, New York.

Sckopke, N. (1966), A general relation between the energy of trapped particles and the disturbance field near Earth, *J. Geophys. Res.*, *71*, 3125.

Seki, K., Y. Miyoshi, D. Summers, and N. P. Meredith (2005), Comparative study of outer-zone relativistic electrons observed by Akebono and CRRES, *J. Geophys. Res.*, *110*, A02203, doi:10.1029/2004JA010655.

Shprits, Y. Y., R. M. Thorne, R. B. Horne, S. A. Glauert, M. Cartwright, C. T. Russell, D. N. Baker, and S. G. Kanekal (2006), Acceleration mechanism responsible for the formation of the new radiation belt during the 2003 Halloween solar storm, *Geophys. Res. Lett.*, *33*, L05104, doi:10.1029/2005GL024256.

Smart, D. F., M. A. Shea, and E. O. Fluckiger (2000), Magnetospheric models and trajectory computations, *Space Sci. Rev.*, *93*, 305.

Vampola, A. L. (1996), The ESA outer zone electron model update, in *Environment Modelling for Space-Based Applications*, edited by W. Burke and T.-D. Guyenne, *Eur. Space Agency Spec. Publ., ESA SP-392*, 151–158.

Wygant, J., F. Mozer, M. Temerin, J. Blake, N. Maynard, H. Singer, and M. Smiddy (1994), Large amplitude electric and magnetic field signatures in the inner magnetosphere during injection of 15 MeV electron drift echoes, *Geophys. Res. Lett.*, *21*, 1739.

J. Albert, Space Vehicles Directorate, Air Force Research Laboratory, 29 Randolph Road, Hanscom Air Force Base, MA 01731-3010, USA.

C. C. Goodrich and J. G. Lyon, Center for Integrated Space Weather Modeling, Boston University, 725 Commonwealth Avenue, Boston, MA 02155, USA.

M. K. Hudson and B. T. Kress, Department of Physics and Astronomy, Dartmouth College, 6127 Wilder Laboratory, Hanover, NH 03755, USA. (bkress@northstar.dartmouth.edu)

M. D. Looper, Space Sciences Department, Aerospace Corporation, P. O. Box 92957, M2/260, Los Angeles, CA 90009-2957, USA.